Total (elastic plus inelastic) cross sections for electron scattering with argon and krypton atoms at energies 10-6000 eV

1990 Phys. Scr. 41 321

(http://iopscience.iop.org/1402-4896/41/3/005)

Physica Scripta. Vol. 41, 321–328, 1990.

Total (Elastic Plus Inelastic) Cross Sections for Electron Scattering with Argon and Krypton Atoms at Energies 10–6000 eV

Ashok Jain*, B. Etemadi* and K. R. Karim**

*Physics Department, Florida A & M University Tallahassee, FL 32307, U.S.A.; **Physics Department, Illinois State University, Normal, IL 61761, U.S.A.

Received May 29, 1989; accepted August 15, 1989

Abstract

Total cross sections (elastic plus inelastic) are reported for electron–Ar and Kr scattering at energies 10–6000 eV. A model complex-optical-potential (COP) approach is employed in which the real and imaginary parts are expressed in terms of the target electron density. For the real part of the COP, the static potential is determined exactly at the Hartree–Fock level, the exchange potential is approximated in the free-electron-gas model and the polarisation effects are included via the parameter-free correlation polarisation potential. The imaginary part of the COP, i.e. the absorption potential, is a function of projectile energy, target charge density, mean excitation energy of the atom, and static and the exchange potential terms. The charge density of the atom is obtained accurately from the numerical self-consistent Hartree–Fock procedure. The complex potential scattering problem is solved exactly under the variable-phase-approach. Our total cross sections compare very well with the measured values at all energies considered here. We also present differential cross sections (DCS) with and without absorption effects. We found that absorption effects improve the elastic DCS at all energies above the excitation threshold.

1. Introduction

Recently, total cross sections (σ_t) for scattering of electrons from Ar and Kr atoms have been measured by Garcia *et al.* [1] at 700–6000 eV. More recently, differential cross sections (DCS) for the e-Kr system have been measured by Danjo [2] in the range 5–200 eV from 10 to 125°, while Weyhreter *et al.* [3] have measured the e–Ar and Kr DCS at very low energies (0.05–2 eV). For the e–Ar scattering there are a large number of experimental and theoretical studies for both the total and DCS scattering parameters (for a comprehensive list of publications see Refs. [4–6]). Garcia *et al.* [1] have provided a list of earlier measurements and calculations on both the targets (Ar and Kr) in the intermediate and high energy regions. However, most of the e–Ar theoretical studies have been devoted mainly to the elastic scattering (neglecting the effects of inelastic channels). In addition, there is a paucity of total cross section calculations at high energies (above 500 eV). To the best of our knowledge, there is no calculation for the σ_t on these atoms above the few keV energy region. In the present work, we report σ_t values for both the e–Ar and Kr collisions in a wide energy range (10–6000 eV) where very recent experimental data are available for comparison. Very recently, Nishimura and Yano [7] have also measured total cross sections for the e-Ar system at 7–500 eV.

In order to evaluate the σ_t cross sections, the optical potential of the electron–atom system must be complex; the imaginary part of the complex optical potential (known as the absorption potential) takes into account the flux going into all the possible inelastic channels. Thus, the inclusion of absorption effects into any model potential calculation reduces the elastic DCS. These are the DCS (modified DCS, to be represented by MDCS) which should be compared with the experimental pure elastic DCS. Recently, Hasenburg *et al.* [8] have found that the inclusion of local absorption interaction to consider the loss of flux into inelastic channels improves the agreement with experimental elastic DCS. Similar observations have been seen in the case of positron–atom collisions [9, 10]. Hence, in a total cross section calculation, where absorption effects are included, it becomes important and interesting to look into the elastic MDCS and compare them with the corresponding experimental data. In this work, we also found that the MDCS (with absorption effects) compare better than the usual DCS (without absorption) with experiments for both the Ar and Kr targets.

The only other calculations at such high impact energies are due to Joachain *et al.* [11] who calculated the total cross sections for electron-argon scattering at 700, 800 and 1000 eV using a model optical potential approach, and of de Heer *et al.* [12] who employed semiempirical methods to obtain σ_t at energies 1–3 keV. McCarthy *et al.* [13] have reported optical potential DCS results for the e–Kr scattering up to few hundred eV energies only. Walters [14] has reviewed all previous theoretical work related with such calculations at intermediate and high energies. Note that for the electron–Kr system, as compared to the Ar case, there is less theoretical work available in the literature.

It is to be noted here that unlike the elastic scattering process, the evaluation of total cross sections (elastic plus all possible inelastic channels) becomes very difficult due to the infinite number of possible states. The method of complex-optical-potential (COP), in which the imaginary part takes care of the loss of flux due to all possible inelastic channels, has been found to be very successful for intermediate and high energy collisions. Although an exact determination of the complex potential is a formidable task, a number of empirical and semiempirical schemes have been quite promising [14, 15]. Our imaginary part of the COP uses basically the same expression [16] as described by Truhlar and coworkers [15].

In the next section, we give a summary of our theoretical model and in Section 3 the numerical details are provided. The results are discussed in Section 4 and finally the conclusions are presented in the last section. We use atomic units throughout this paper.

2. Theoretical model

We simplify the electron–atom scattering problem by replacing the interaction between the projectile and the target by a local optical potential. In a scattering problem, above the first ionization threshold, this potential is complex and is written as

$$V_{opt}(r) = V_R(r) + iV_{abs}(r), \tag{1}$$

where the real part is given by

$$V_R(r) = V_{st}(r) + V_{ex}(r) + V_p(r). \tag{2}$$

Here $V_{st}(r)$, $V_{ex}(r)$, and $V_p(r)$ are, respectively, the static, exchange and polarization interactions, and V_{abs} is the absorption potential. The static potential is calculated accurately from

$$V_s(r) = \frac{Z}{r} - \int \frac{\varrho_0(r')\,d^3r'}{|r - r'|}. \tag{3}$$

where $\varrho_0(r)$ is the target unperturbed charge density. The exchange potential is taken to be the HFEGE (free-electron-gas-exchange, Hara type) potential [17],

$$V_{ex}(r) = \frac{2}{\pi} k_f(r) \left[\frac{1}{2} + \frac{1-\eta}{4\eta} \ln\left|\frac{1+\eta}{1-\eta}\right|\right], \tag{4}$$

where

$$k_f(r) = [3\pi^2 \varrho_0(r)]^{1/3}, \tag{5}$$

and

$$\eta(r) = (k^2 + 2I + k_f^2)^{1/2}/k_f. \tag{6}$$

Here I is the ionization potential of the outermost orbital of the atom. This version of the HFEGE potential does not give correct asymptotic behaviour. We, therefore, choose $I = 0$, in eq. (6); this is the so called asymptotically adjusted HFEGE potential.

The long-range part of the polarization potential is taken as the following well known asymptotic form,

$$V_p(r) = -\frac{\alpha_d}{2r^4}, \quad r > r_c \tag{7}$$

where α_d is the electric dipole polarizability of the target atom. In the short range, $r \leqslant r_c$, the V_p is represented by the correlation polarization (COP) potential first introduced by O'Connel and Lane [18],

$$\begin{aligned} V_p(r) &= 0.0622 \ln r_s - 0.096 + 0.018 r_s \ln r_s - 0.02 r_s, \\ &\qquad r_s \leqslant 0.7 \\ &= -0.1231 + 0.037\,96 \ln r_s, \quad 0.7 \leqslant r_s \leqslant 10 \\ &= -0.876 r_s^{-1} + 2.65 r_s^{-3/2} - 2.8 r_s^{-2} - 0.8 r_s^{-5/2}, \\ &\qquad 10 \leqslant r_s \end{aligned} \tag{8}$$

where $r_s = (3/4\pi\varrho_0)^{1/3}$ and the parameter r_c [eq. (7)] is the first crossing point of the COP [eq. (8)] and asymptotic [eq. (7)] polarisation potentials.

For the imaginary part of the optical potential we use the absorption potential discussed by Truhlar and co-workers [15]

$$\begin{aligned} V_{abs}(r) &= -\varrho_0(r)(v_{loc}/2)^{1/2}(8\pi^2/10k_f^3 E) H(2k^2 - k_f^2 - 2\Delta) \\ &\quad \times (A_1 + A_2 + A_3), \end{aligned} \tag{9}$$

where

$$\begin{aligned} v_{loc}(r) &= k^2 - V_{st}(r) - V_{ex}(r), \\ A_1 &= 5k_f^3/2\Delta, \\ A_2 &= -k_f^3(5k^2 - 3k_f^2)/(2k^2 - k_f^2), \end{aligned} \tag{10}$$

and

$$A_3 = H(2k_f^2 + 2\Delta - 2k^2)(2k_f^2 + 2\Delta - 2k^2)^{5/2}. \tag{11}$$

The mean excitation energy Δ is calculated from,

$$\Delta = \frac{2\langle\psi_0|z^2|\psi_0\rangle}{\alpha_d} \tag{12}$$

where ψ_0 is the ground-state wave function of the target atom. The Heaviside function $H(x)$ in eqs. (9) and (11) is defined as

$$H(x) = \begin{cases} 1, & x \geqslant 0 \\ 0, & x < 0. \end{cases} \tag{13}$$

The optical potential [eq. (1)] with various real and imaginary terms [eqs. (3)–(9)] is quite easy to calculate once the charge density of the target is known. In addition, it does not involve any fitting parameter except the fact that the mean excitation energy can be chosen approximately. Finally, the choice of our optical potential is justified by the fact that all the cross section results reported here compare very well with measured data at all energies considered here. Finally, we solve the following radial Schrödinger equation under the complex-optical-potential, $V_{opt}(r)$,

$$\frac{d^2u_l(r)}{dr^2} + \left[k^2 - \frac{l(l+1)}{r^2} - 2V_{opt}(r)\right] u_l(r) = 0, \tag{14}$$

where $k^2/2$ is the energy of the particle. The scattering wavefunction ψ can be expressed in terms of $u_l(r)$ as

$$\begin{aligned} \psi &= \sum_l A_l P_l(\cos\theta) \sqrt{\frac{\pi}{2}}\, u_l(r)/kr \\ &\equiv \frac{1}{2ikr} \sum_l i^l (2l+1) P_l(\cos\theta) [e^{-i(kr - l\pi/2)} + S_l(k)\, e^{i(kr - l\pi/2)}], \end{aligned} \tag{15}$$

where

$$S_l(k) = e^{2i(\delta_l + i\beta_l)} \tag{16}$$

is the scattering matrix defined in terms of the complex phase-shift $(\delta_l + i\beta_l)$. It is now straightforward to deduce the expressions for the elastic, absorption and total cross sections in terms of the S-matrix:

$$\sigma_{el} = \sum_{l=0}^{l_{max}} \frac{\pi}{k^2} (2l+1) |1 - S_l(k)|^2, \tag{17}$$

$$\sigma_{abs} = \sum_{l=0}^{l_{max}} \frac{\pi}{k^2} (2l+1)[1 - |S_l(k)|^2], \tag{18}$$

and

$$\sigma_t = \sigma_{el} + \sigma_{abs} = \sum_{l=0}^{l_{max}} \frac{2\pi}{k^2} (2l+1)[1 - \mathrm{Re}\, S_l(k)]. \tag{19}$$

The DCS are calculated from,

$$\frac{d\sigma}{d\Omega} = \frac{1}{4k^2} \left| \sum_{l=0}^{l_{max}} (2l+1)[S_l(k) - 1] P_l(\cos\theta) \right|^2, \tag{20}$$

where $P_l(\cos\theta)$ is a Legendre polynomial of order l and the momentum transfer (σ_m) cross sections are evaluated from the integration of eq. (20) with a weighting factor of $[1 - \cos\theta]$.

3. Numerical details

We generated the bound-state orbitals, $P_{nl}(r)$, of neutral argon and krypton atoms by solving numerically the Hartree–Fock equation [19]. The electron density function $\varrho_0(r)$ in eq. (3) was then obtained in terms of these orbitals as

$$\varrho_0(r) = \sum_{nl} q_{nl} P_{nl}^2(r), \tag{21}$$

where q_{nl} is the number of electrons in subshell nl. The $\varrho_0(r)$ [eq. (21)] was used to calculate all the potentials, $V_{st}(r)$, $V_{ex}(r)$, $V_p(r)$, and $V_{abs}(r)$ as described in Section 2. The ionization potentials I of the outer most orbitals of Ar and Kr atoms were calculated as $I = E_0 - E_0^+$ where E_0 is the total energy of the neutral argon or krypton atom and E_0^+ is that of singly ionized atom in the outer most subshell. We have recently compared [4] the electron density function for the argon atom obtained using the wave functions of Clementi and Roetti [20] and the static potential obtained from parametric expressions of Cox and Bonham [21] with the corresponding quantities obtained from the present *ab initio* Hartree–Fock approach. The various potential terms for the e–Ar case are already shown in our earlier publication [4]. Here we provide only the absorption potential terms in Fig. 1 for both the Ar and Kr atoms at 100 eV only. From Fig. 1, we see that the absorption effects exist only in the outer region of the target, however, the range of the V_{abs} is not as large as of the polarisation potential.

The scattering eq. (14) was solved numerically using the variable-phase-technique [22] and the converged phase-shifts (up to an accuracy of 0.00001) were extracted for each energy and partial wave. Our final cross sections are converged numerically within the 0.00001 accuracy. The values of the polarisibilities employed here for both the atoms are as follows: $\alpha_d^{Ar} = 11.08$ a.u., $\alpha_d^{Kr} = 16.8$ a.u.

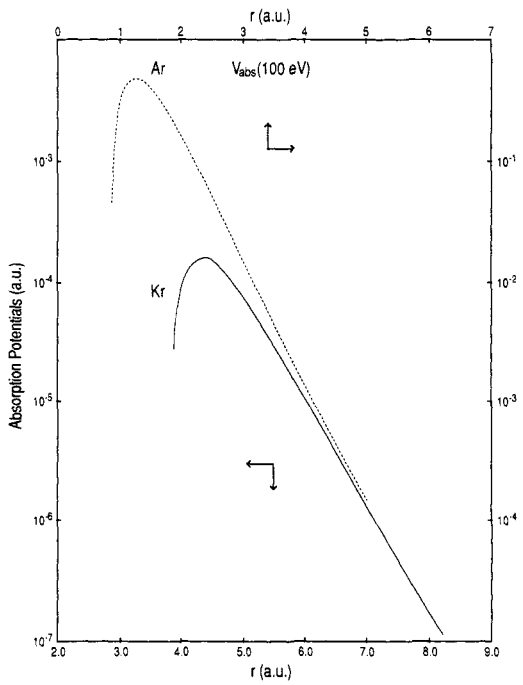

Fig. 1. The negative of the imaginary part (V_{abs}) of the optical potentials for the e–Ar (solid curve) and e–Kr (dash curve) systems at 100 eV.

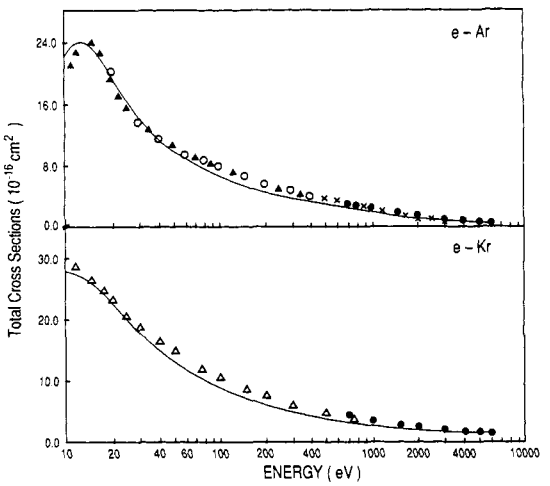

Fig. 2. Total (elastic plus inelastic) cross sections (in units of 10^{-16} cm^2) for the e–Ar and e–Kr collision systems in the range 10–6000 eV. The calculations are shown by solid curves, while the expt. data are as follows: Solid circles, Ref. [1] for both the Ar and Kr; Open circles, Ref. [24] for Ar; Open triangles, Refs. [26] and [27] for Kr; Crosses, Ref. [23] for Ar; Solid triangles, Ref. [7] for Ar.

4. Results and discussion

Our σ_t cross sections for both the e–Ar and e–Kr systems are shown in Fig. 2. Also shown in this figure are the experimental data of Garcia *et al.* [1], Nogueira *et al.* [23], Wagenaar [24], Kauppila *et al.* [25], Dababneh *et al.* [26, 27] and Nishimura and Yano [7]. In Table I, we have provided our σ_t values for the e–Ar case along with the pure elastic (σ_{el}) and inelastic (σ_{abs}) cross sections in the present energy region. Table II presents similar data for the Kr atom. From Fig. 2,

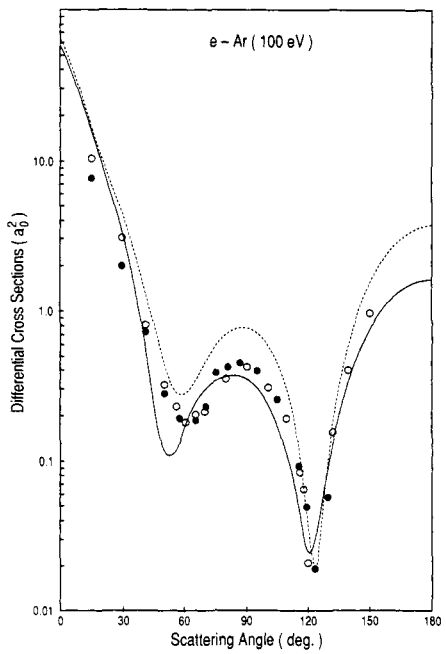

Fig. 3. The differential cross sections for the e–Ar elastic scattering at 100 eV. The theoretical curves represent with (solid curve) and without (dash line) absorption effects. The experimental data are due to Williams and Willis [29] (solid circles) and Srivastava *et al.* [28] (open circles).

Table I. *Elastic (σ_{el}), absorption (σ_{abs}), and total cross section (σ_t) in units of Å^2 for e–Ar scattering at 10–6000 eV. The σ'_{el} is the elastic scattering cross section without absorption effects*

E (eV)	σ'_{el}	σ_{el}	σ_{abs}	σ_t	Ref. [1]	Ref. [7][a]	Ref. [25]	Ref. [6]	Ref. [12]
10	22.53	22.53	0.00	22.53	–	18.7[a]	–	–	–
15	23.74	23.74	0.00	23.74	–	24.3[a]	–	–	–
20	19.80	19.79	0.02	19.81	–	19.6[a]	20.18	–	21.86
30	14.92	13.69	4.95	14.19	–	14.10[a]	12.90	13.89	16.30
40	10.87	10.35	1.07	11.42	–	12.10[a]	–	11.83	12.73
50	9.11	8.35	1.52	9.88	–	11.0[a]	9.92	10.22	11.12
60	7.96	7.05	1.85	8.90	–	9.84[a]	–	9.46	10.22
80	6.55	5.43	2.22	7.65	–	9.04[a]	–	8.71	8.98
100	5.68	4.32	2.44	6.76	–	7.82[a]	7.65	8.11	8.26
200	3.80	2.50	2.13	4.63	–	5.76[a]	5.60	5.84	5.97
300	3.05	2.06	1.69	3.75	–	4.59[a]	4.59	4.78	4.70
400	2.61	1.79	1.41	3.20	–	3.87[a]	–	4.08	3.99
500	2.31	1.59	1.22	2.81	–	3.27[a]	3.31	3.58	3.50
700	1.90	1.32	0.97	2.29	3.05	3.23[b]	2.72	2.97	–
800	1.76	1.21	0.88	2.09	2.84	3.03[b]	2.54	–	–
1000	1.53	1.05	0.76	1.81	2.41	2.66[b]	–	–	2.22
2000	0.97	0.69	0.45	1.14	1.41	1.33	–	–	1.35
3000	0.73	0.54	0.32	0.86	1.03	0.92[b]	–	–	0.97
4000	0.58	0.45	0.25	0.70	0.73	–	–	–	–
5000	0.49	0.39	0.21	0.60	0.61	–	–	–	–
6000	0.42	0.34	0.18	0.52	0.56	–	–	–	–

it is clear that the present results for both the targets on the σ_t parameter compare reasonably well with all the displayed experimental points at higher as well as at lower ends of the present energy regime. Note that basically we have not fitted anything except to adjust little bit the value of the mean excitation energy (Δ = 18.0 eV for both the target atoms). The low-energy hump is clearly visible in our calculated curves. Below 15 eV, some discrepancy exists between theory and experiment; this is expected since at such low energies we need an accurate description of exchange and polarisation forces rather than treating them via model potentials. In Fig. 2, we have not shown the error bars of the experimental points. We mention here that most of our cross sections lie within the error bars of the measured data. This is encouraging since basically we have not employed any phenomenological approach. All the potential terms (real and imaginary) do not involve any adjustable free parameter.

The effect of including the V_{abs} interaction is to decrease the DCS (and consequently the σ_{el} and σ_m) values; we notice that this reduction is appreciable at intermediate energies. For example, from Tables I and II, we can see the difference between the elastic cross sections with (σ_{el}) and without (σ'_{el}) absorption effects. At these higher energies ($E \geqslant 100$ eV) it really does not matter what approximation we use for exchange and polarisation interactions.

Table II. *Elastic (σ_{el}), absorption (σ_{abs}), and total cross section (σ_t) in units of Å^2 for electron–Kr scattering at 10–6000 eV. The quantity σ'_{el} is the elastic scattering cross section without the absorption effects*

E (eV)	σ'_{el}	σ_{el}	σ_{abs}	σ_t	Ref. [1]	Ref. [27]
10	27.84	27.84	0.00	27.84	–	–
20	22.34	22.33	0.02	22.36	–	23.10
30	17.20	16.91	0.61	17.52	–	18.60
40	14.23	13.52	1.31	14.84	–	16.05
50	12.32	11.25	1.87	13.12	–	14.4
60	10.92	9.55	2.28	11.83	–	–
80	8.95	7.01	2.82	9.83	–	11.70
100	7.65	5.44	3.03	8.46	–	10.44
150	5.85	3.89	2.81	6.70	–	8.55
200	4.94	3.26	2.50	5.76	–	7.39
300	3.96	2.63	2.04	4.67	–	5.97
400	3.44	2.29	1.73	4.02	–	5.07
500	3.07	2.01	1.53	3.54	–	4.47
600	2.79	1.82	1.38	3.20	–	4.01
800	2.40	1.53	1.17	2.70	3.91	3.42
1000	2.13	1.33	1.02	2.35	3.32	–
2000	1.43	0.93	0.65	1.58	1.69	–
3000	1.12	0.77	0.48	1.25	1.75	–
4000	0.94	0.66	0.39	1.05	1.46	–
5000	0.81	0.59	0.33	0.92	1.23	–
6000	0.72	0.53	0.28	0.81	1.09	–

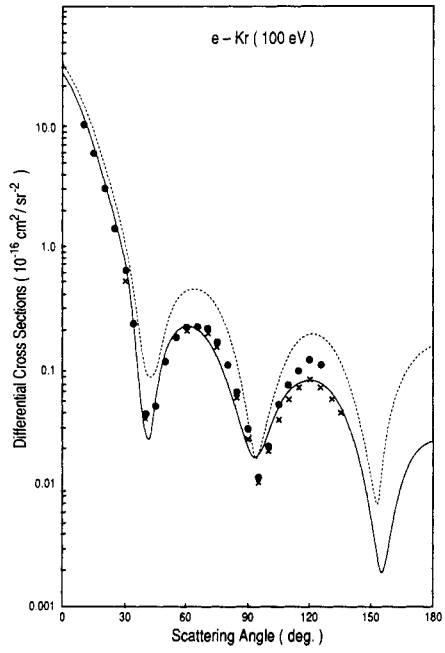

Fig. 4. Same caption as in Fig. 4, except for the e–Kr collision system. The experimental points are due to Danjo [2] (solid circles) and Srivastava *et al.* [28] (crosses).

We now discuss our DCS for both the targets. In Figs. 3 and 4, we have plotted the present e–Ar and e–Kr DCS and MDCS at 100 eV along with several sets of experimental points. We see a clear improvement in the MDCS curves relative to the corresponding DCS curves for both the systems. A similar situation exists at other energies (not shown) also. As expected the DCS (without absorption effects) curves overestimate the experimental data at all angles. When we compare both sets of differential curves (DCS and MDCS) with the measured results (from Refs. [2, 28, 29]) for both the scattering systems (Ar and Kr), we see that the MDCS are in better accord than the corresponding DCS results. In particular, the structure of the dips and humps (both in magnitude and width) improves significantly when the absorption effects are switched on. Note that the differential cross sections for the e–Kr system are more rich in structure; our MDCS curve (Fig. 5) is in good agreement with the measurements of Srivastava *et al.* [28] and Danjo [2]. Due to crowded points we have not shown the measurements of Williams and Crowe [30], Jansen and Heer [31], Jansen *et al.* [32], Bromberg [33], Wagenaar and Heer [34], Dubois and Rudd [35], Williams [36] and Wagenaar *et al.* [6]. In addition, we did not include in these figures (3 and 4) several calculations due to Haberland *et al.* [37], Barstchat *et al.* [10], Hasenburg *et al.* [8], Joachain *et al.* [11], McCarthy *et al.* [13], etc. for both the scattering systems considered here. All the calculations prior to 1978 on these systems have been reviewed by Bransden and McDowell [38]. Our list of earlier references (both experimental and theoretical) is not complete.

Finally, in order to make these calculations available to other investigators, we have listed the present MDCS for both the targets, i.e., Ar and Kr, in Tables III and IV respectively (only at some selected energies; for other energies, these tables are available from the authors at request).

The momentum transfer cross sections can easily be calculated by the integration of the MDCS as discussed in Section 2. Our σ_m values for both the Ar and Kr atoms are plotted in Fig. 5 in the present energy range. In this figure

Table III. (*a*) *Elastic differential cross sections in units of* 10^{-16} *cm*^{2} *for scattering of electrons by Ar atoms at several impact energies. A number, for example, 1.435 + 1, means 1.435* $\times$ 10^{+1}

	Energy in eV						
Angle	20	40	50	60	100	200	300
0	1.435+1	1.286+1	1.363+1	1.458+1	1.593+1	1.809+1	2.029+1
5	1.360+1	1.096+1	1.115+1	1.136+1	1.127+1	1.075+1	1.079+1
10	1.232+1	8.838+0	8.573+0	8.405+0	7.476+0	5.955+0	5.263+0
15	1.102+1	7.089+0	6.484+0	6.090+0	4.804+0	3.133+0	2.424+0
20	9.643+0	5.639+0	4.847+0	4.321+0	2.948+0	1.535+0	1.034+0
25	8.212+0	4.411+0	3.553+0	2.982+0	1.701+0	6.875−1	4.170−1
30	6.763+0	3.364+0	2.532+0	1.986+0	9.070−1	2.866−1	1.845−1
35	5.355+0	2.473+0	1.736+0	1.262+0	4.369−1	1.257−1	1.080−1
40	4.030+0	1.727+0	1.122+0	7.499−1	1.862−1	7.312−2	7.747−2
45	2.861+0	1.117+0	6.669−1	4.042−1	7.173−2	5.719−2	5.735−2
50	1.877+0	6.442−1	3.464−1	1.850−1	3.349−2	4.975−2	4.237−2
55	1.108+0	3.083−1	1.395−1	6.273−2	3.291−2	4.383−2	3.229−2
60	5.637−1	9.967−2	3.140−2	1.392−2	4.709−2	3.894−2	2.534−2
65	2.313−1	8.293−3	3.230−3	1.742−2	6.506−2	3.467−2	2.038−2
70	8.933−2	1.367−2	3.578−2	5.691−2	8.172−2	3.038−2	1.688−2
75	9.090−2	9.121−2	1.094−1	1.173−1	9.480−2	2.574−2	1.396−2
80	1.894−1	2.118−1	2.041−1	1.855−1	1.025−1	2.083−2	1.128−2
85	3.340−1	3.473−1	3.003−1	2.496−1	1.034−1	1.587−2	8.881−3
90	4.800−1	4.716−1	3.821−1	2.985−1	9.740−2	1.108−2	6.623−3
95	5.904−1	5.627−1	4.368−1	3.253−1	8.460−2	6.747−3	4.911−3
100	6.467−1	6.079−1	4.541−1	3.260−1	6.665−2	3.389−3	4.048−3
105	6.399−1	5.998−1	4.340−1	2.997−1	4.659−2	1.491−3	3.959−3
110	5.818−1	5.432−1	3.817−1	2.515−1	2.760−2	1.453−3	4.789−3
115	4.908−1	4.483−1	3.028−1	1.900−1	1.315−2	3.558−3	6.645−3
120	3.956−1	3.297−1	2.127−1	1.257−1	6.687−3	7.919−3	9.401−3
125	3.304−1	2.093−1	1.284−1	7.064−2	1.083−2	1.442−2	1.310−2
130	3.194−1	1.045−1	6.143−2	3.622−2	2.741−2	2.296−2	1.747−2
135	3.878−1	3.147−2	2.558−2	3.082−2	5.688−2	3.312−2	2.209−2
140	5.427−1	2.157−3	2.830−2	5.924−2	9.843−2	4.453−2	2.722−2
145	7.839−1	2.007−2	7.124−2	1.208−1	1.502−1	5.659−2	3.261−2
150	1.096+0	8.227−2	1.511−1	2.112−1	2.085−1	6.871−2	3.719−2
155	1.450+0	1.779−1	2.552−1	3.218−1	2.693−1	8.049−2	4.188−2
160	1.813+0	2.930−1	3.730−1	4.378−1	3.285−1	9.092−2	4.633−2
165	2.148+0	4.083−1	4.896−1	5.471−1	3.804−1	9.984−2	4.939−2
170	2.418+0	5.064−1	5.825−1	6.389−1	4.205−1	1.064−1	5.158−2
175	2.593+0	5.732−1	6.445−1	6.971−1	4.471−1	1.107−1	5.367−2
180	2.654+0	5.916−1	6.723−1	7.167−1	4.572−1	1.129−1	5.499−2
σ_m	9.75	4.29	2.84	1.39	0.45	0.29	0.21

Table III. (*b*) *Elastic differential cross sections in units of* 10^{-16} *cm*^{2} *for scattering of electrons by Ar atoms at several impact energies. A number, for example, 1.435+1, means* $1.435 \times 10^{+1}$

	Energy in eV						
Angle	400	500	600	800	1000	2000	3000
0	2.195+1	2.325+1	2.423+1	2.603+1	2.741+1	3.103+1	3.333+1
5	1.066+1	1.039+1	1.012+1	9.412+0	8.775+0	6.713+0	5.429+0
10	4.698+0	4.192+0	3.776+0	3.085+0	2.579+0	1.351+0	8.749−1
15	1.956+0	1.603+0	1.348+0	9.686−1	7.324−1	3.356−1	2.318−1
20	7.624−1	5.868−1	4.780−1	3.400−1	2.691−1	1.464−1	1.004−1
25	3.066−1	2.491−1	2.178−1	1.749−1	1.500−1	7.765−2	4.366−2
30	1.589−1	1.437−1	1.324−1	1.086−1	8.986−2	3.843−2	2.069−2
35	1.038−1	9.386−2	8.337−2	6.523−2	5.444−2	1.851−2	8.551−3
40	7.065−2	6.077−2	5.234−2	3.873−2	2.803−2	8.924−3	4.626−3
45	4.808−2	3.899−2	3.158−2	2.044−2	1.561−2	4.257−3	2.239−3
50	3.299−2	2.496−2	1.907−2	1.217−2	8.419−3	2.363−3	1.398−3
55	2.337−2	1.664−2	1.267−2	8.037−3	5.759−3	1.347−3	8.510−4
60	1.752−2	1.257−2	9.864−3	6.518−3	4.752−3	8.586−4	5.434−4
65	1.428−2	1.054−2	8.924−3	6.038−3	4.049−3	5.662−4	4.020−4
70	1.217−2	9.494−3	7.891−3	5.534−3	3.883−3	4.027−4	2.648−4
75	1.052−2	8.542−3	7.683−3	5.112−3	3.218−3	2.878−4	2.276−4
80	9.039−3	7.623−3	6.455−3	4.509−3	2.967−3	2.348−4	1.720−4
85	7.604−3	6.646−3	5.846−3	3.823−3	2.403−3	1.975−4	1.512−4
90	6.340−3	5.533−3	4.872−3	3.323−3	2.168−3	1.858−4	1.375−4
95	5.278−3	4.876−3	4.222−3	2.755−3	1.849−3	1.859−4	1.211−4
100	4.673−3	4.300−3	3.584−3	2.524−3	1.737−3	1.928−4	1.208−4
105	4.618−3	4.095−3	3.460−3	2.220−3	1.609−3	2.086−4	1.176−4
110	5.117−3	4.270−3	3.273−3	2.244−3	1.646−3	2.231−4	1.098−4
115	6.172−3	4.724−3	3.678−3	2.231−3	1.660−3	2.435−4	1.238−4
120	7.736−3	5.539−3	3.992−3	2.484−3	1.819−3	2.583−4	1.074−4
125	9.757−3	6.627−3	4.783−3	2.752−3	1.952−3	2.802−4	1.283−4
130	1.211−2	7.961−3	5.624−3	3.172−3	2.221−3	2.938−4	1.158−4
135	1.476−2	9.488−3	6.722−3	3.696−3	2.424−3	3.074−4	1.241−4
140	1.753−2	1.116−2	7.931−3	4.245−3	2.760−3	3.266−4	1.320−4
145	2.034−2	1.295−2	9.231−3	4.926−3	3.022−3	3.293−4	1.192−4
150	2.314−2	1.466−2	1.060−2	5.495−3	3.341−3	3.502−4	1.469−4
155	2.568−2	1.641−2	1.184−2	6.177−3	3.589−3	3.495−4	1.220−4
160	2.802−2	1.794−2	1.313−2	6.678−3	3.863−3	3.597−4	1.499−4
165	2.987−2	1.920−2	1.401−2	7.197−3	4.057−3	3.709−4	1.336−4
170	3.138−2	2.027−2	1.494−2	7.518−3	4.204−3	3.583−4	1.356−4
175	3.221−2	2.083−2	1.525−2	7.747−3	4.313−3	3.895−4	1.579−4
180	3.248−2	2.086−2	1.568−2	7.909−3	4.354−3	3.108−4	9.137−5
σ_m	0.21	0.16	0.13	0.082	0.058	0.016	0.0096

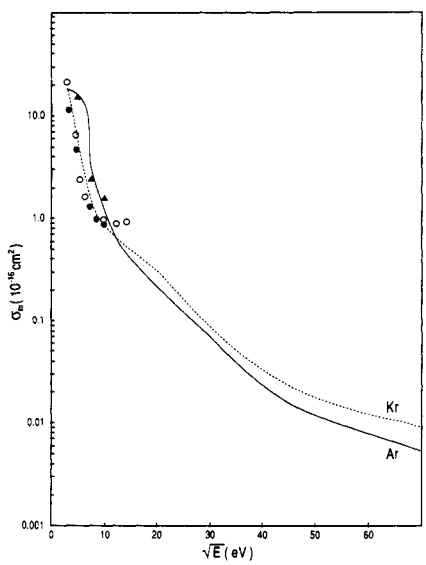

Fig. 5. Momentum transfer (σ_m) (in units of Å^2) cross sections for both the e–Ar (solid line) and e–Kr (dash line) systems at 10–6000 eV. The experimental points (solid triangles) for the e–Ar are from Srivastava *et al.* [28]; for e–Kr case, open circles are the measurements of Danjo [2] and the solid circles from Srivastava *et al.* [28].

we have also shown the measured results of Danjo [2] and Srivastava *et al.* [28] available at low energies (below 200 eV) only. However, even in this narrow energy region, we see a good agreement between our results and these experimental values. The two σ_m values at 150 and 200 eV of Danjo [2] seem to be rather strange. In general, the σ_m curves are decreasing monotonically throughout the energy range; however, the flat behaviour of Danjo [2] σ_m values beyond 100 eV is quite different from ours as well as the observations of Srivastava *et al.* [28]. At low energies, the argon σ_m cross sections are higher than the corresponding krypton values (a fact also observed by Srivastava *et al.* [28]); however, above 100 eV, the Kr momentum transfer cross sections are larger than the corresponding Ar data.

5. Conclusions

We have reported elastic differential, integral, momentum transfer and total (elastic plus inelastic) cross sections in a parameter-free model complex-optical-potential approach in a wide energy range 10–6000 eV. These calculations are compared with available experimental data and were found to be

Table IV. (*a*) *Same details as in Table III(a), but for the Kr atom*

	Energy in eV						
Angle	20	40	50	60	100	200	300
0	2.466+1	3.146+1	3.234+1	2.902+1	3.062+1	3.335+1	3.578+1
5	2.262+1	2.651+1	2.552+1	2.015+1	1.695+1	1.609+1	1.545+1
10	1.922+1	2.071+1	1.861+1	1.256+1	8.452+0	6.944+0	5.970+0
15	1.611+1	1.497+1	1.208+1	7.083+0	3.880+0	2.782+0	2.172+0
20	1.290+1	1.022+1	7.545+0	3.758+0	1.594+0	1.015+0	7.630−1
25	1.005+1	6.782+0	4.403+0	1.715+0	5.608−1	3.719−1	3.266−1
30	7.694+0	4.280+0	2.267+0	6.313−1	1.853−1	1.842−1	1.857−1
35	5.744+0	2.494+0	1.003+0	1.516−1	1.001−1	1.252−1	1.084−1
40	4.122+0	1.338+0	3.377−1	2.434−2	9.937−2	9.132−2	6.681−2
45	2.847+0	6.390−1	7.099−2	5.199−2	1.054−1	6.930−2	4.569−2
50	1.893+0	2.694−1	3.399−2	1.303−1	9.966−2	5.335−2	3.489−2
55	1.199+0	1.260−1	1.085−1	1.893−1	8.368−2	3.929−2	2.777−2
60	7.098−1	1.033−1	2.057−1	2.121−1	6.103−2	2.625−2	2.055−2
65	4.010−1	1.465−1	2.837−1	1.989−1	3.663−2	1.527−2	1.389−2
70	2.567−1	2.127−1	3.210−1	1.615−1	1.646−2	7.270−3	8.441−3
75	2.163−1	2.696−1	3.134−1	1.142−1	3.564−3	3.838−3	6.097−3
80	2.430−1	3.092−1	2.743−1	6.969−2	4.815−5	4.912−3	6.185−3
85	3.065−1	3.262−1	2.162−1	3.720−2	5.099−3	9.597−3	8.268−3
90	3.818−1	3.228−1	1.536−1	1.949−2	1.610−2	1.596−2	1.102−2
95	4.439−1	3.063−1	9.710−2	1.810−2	3.034−2	2.175−2	1.311−2
100	4.850−1	2.778−1	5.360−2	2.838−2	4.292−2	2.572−2	1.379−2
105	5.031−1	2.411−1	2.418−2	4.389−2	5.235−2	2.610−2	1.262−2
110	4.996−1	2.047−1	7.889−3	6.096−2	5.475−2	2.374−2	9.963−3
115	4.718−1	1.650−1	1.324−3	7.142−2	5.210−2	1.854−2	6.498−3
120	4.349−1	1.223−1	6.716−4	7.712−2	4.361−2	1.261−2	3.212−3
125	4.144−1	8.663−2	2.512−3	7.136−2	3.283−2	7.442−3	1.372−3
130	4.116−1	5.460−2	5.775−3	6.083−2	2.195−2	4.986−3	2.108−3
135	4.320−1	2.624−2	1.045−2	4.462−2	1.423−2	6.836−3	6.175−3
140	4.743−1	9.011−3	1.638−2	2.789−2	1.178−2	1.349−2	1.435−2
145	5.535−1	1.780−3	2.764−2	1.467−2	1.590−2	2.575−2	2.626−2
150	6.675−1	5.039−3	4.202−2	5.092−3	2.706−2	4.224−2	4.198−2
155	7.929−1	1.804−2	6.140−2	2.407−3	4.311−2	6.240−2	5.921−2
160	9.179−1	3.571−2	8.504−2	4.553−3	6.344−2	8.285−2	7.788−2
165	1.029+0	5.786−2	1.058−1	1.014−2	8.229−2	1.033−1	9.426−2
170	1.128+0	8.047−2	1.273−1	1.719−2	1.004−1	1.184−1	1.086−1
175	1.200+0	9.055−2	1.401−1	2.255−2	1.105−1	1.300−1	1.170−1
180	1.223+0	8.772−2	1.415−1	2.243−2	1.180−1	1.301−1	1.216−1
σ_m	8.21	2.69	1.87	1.45	0.87	0.53	0.39

Table IV. (*b*) *Same details as in Table III(a), but for the Kr atom*

	Energy in eV						
Angle	400	500	600	800	1000	2000	3000
0	3.761+1	3.912+1	4.077+1	4.217+1	4.478+1	5.176+1	5.696+1
5	1.473+1	1.414+1	1.352+1	1.292+1	1.194+1	9.171+0	7.505+0
10	5.157+0	4.553+0	4.052+0	3.612+0	2.949+0	1.610+0	1.172+0
15	1.730+0	1.441+0	1.220+0	1.042+0	8.050−1	4.803−1	3.434−1
20	6.172−1	5.429−1	4.865−1	4.375−1	3.517−1	1.868−1	1.155−1
25	3.005−1	2.748−1	2.469−1	2.167−1	1.705−1	6.850−2	3.676−2
30	1.649−1	1.421−1	1.201−1	1.013−1	6.895−2	2.671−2	1.783−2
35	8.524−2	6.632−2	5.147−2	3.952−2	2.755−2	1.374−2	9.412−3
40	4.658−2	3.404−2	2.568−2	2.014−2	1.454−2	8.419−3	5.305−3
45	3.065−2	2.412−2	1.990−2	1.682−2	1.213−2	5.260−3	2.689−3
50	2.539−2	2.191−2	1.953−2	1.589−2	1.216−2	3.062−3	1.548−3
55	2.232−2	2.043−2	1.709−2	1.471−2	8.802−3	1.901−3	9.874−4
60	1.760−2	1.538−2	1.395−2	1.041−2	7.004−3	1.300−3	7.738−4
65	1.255−2	1.171−2	8.635−3	7.004−3	3.763−3	9.414−4	7.556−4
70	8.389−3	6.494−3	5.539−3	3.830−3	2.412−3	8.062−4	6.981−4
75	5.558−3	4.574−3	3.000−3	2.108−3	1.228−3	6.507−4	6.380−4
80	4.812−3	3.196−3	2.060−3	1.306−3	7.968−4	5.770−4	6.105−4
85	5.221−3	3.165−3	1.849−3	1.078−3	6.246−4	4.831−4	4.796−4
90	6.049−3	3.484−3	1.979−3	1.063−3	5.379−4	4.121−4	4.551−4
95	6.511−3	3.596−3	1.971−3	1.147−3	5.806−4	3.447−4	3.450−4

Table IV. *Continued*

Angle	Energy in eV						
	20	40	50	60	100	200	300
100	6.260−3	3.445−3	1.955−3	1.016−3	5.736−4	2.953−4	3.038−4
105	5.279−3	2.638−3	1.498−3	9.640−4	6.525−4	2.722−4	2.611−4
110	3.497−3	1.865−3	1.045−3	7.075−4	7.036−4	2.662−4	2.346−4
115	1.798−3	6.634−4	5.566−4	6.595−4	9.202−4	3.180−4	2.321−4
120	4.033−4	1.566−4	3.385−4	7.132−4	1.209−3	3.814−4	2.707−4
125	1.698−4	3.201−4	7.520−4	1.271−3	1.791−3	5.007−4	2.709−4
130	1.683−3	1.724−3	2.098−3	2.444−3	2.595−3	6.517−4	3.824−4
135	5.552−3	5.089−3	4.618−3	4.424−3	3.806−3	8.232−4	3.986−4
140	1.203−2	1.044−2	8.621−3	7.272−3	5.305−3	1.030−3	5.356−4
145	2.100−2	1.753−2	1.397−2	1.110−2	7.118−3	1.242−3	5.880−4
150	3.248−2	2.578−2	2.033−2	1.537−2	9.157−3	1.461−3	7.201−4
155	4.514−2	3.671−2	2.778−2	2.040−2	1.125−2	1.682−3	7.720−4
160	5.781−2	4.513−2	3.471−2	2.490−2	1.327−2	1.859−3	9.106−4
165	7.075−2	5.676−2	4.170−2	2.957−2	1.508−2	2.029−3	9.183−4
170	7.936−2	6.170−2	4.696−2	3.275−2	1.645−2	2.156−3	1.066−3
175	8.689−2	6.927−2	5.010−2	3.516−2	1.741−2	2.215−3	1.025−3
180	8.862−2	6.708−2	5.342−2	3.614−2	1.761−2	2.375−3	9.004−4
σ_m	0.30	0.22	0.18	0.11	0.073	0.023	0.015

in good agreement. In particular the hump structure around 15 eV in the electron–Ar σ_t curve is neatly reproduced in our parameter-free model potential calculations (Fig. 2). The differential cross sections are reduced significantly when the absorption interaction (the imaginary part of the COP) is switched on. We found that the modified DCS are improved upon the usual DCS (without absorption) when compared with the measured elastic DCS at higher energies where inelastic channels are important.

Acknowledgements

A part of the work was done at the Kansas State University where it was partially supported by the Division of Chemical Sciences, U.S. Department of Energy. We thank the Florida State University Computing Center for providing computer time. We acknowledge the support by the FSU Supercomputer Computations Research Institute which is partially funded by the U.S. Department of Energy through Contract No. DE-FC05-85ER250000.

References

1. Garcia, G., Arqueros, F. and Campos, J., J. Phys. **B19**, 3777 (1986).
2. Danjo, A., J. Phys. B: At. Mol. Phys. **21**, 3759 (1988).
3. Weyhreter, M., Barzick, B., Mann, A. and Linder, F., Z. Phys. **D7**, 333 (1988).
4. Karim, K. R. and Jain Ashok, Physica Scripta **39**, 238 (1989).
5. Nahar, S. N. and Wadehra, J. M., Phys. Rev. **A35**, 2051 (1987).
6. Wagenaar, R. W., de Boer, A., van Tubergen, Los, J. and de Heer, F. J., J. Phys. B: At. Mol. Phys. **19**, 3121 (1986).
7. Nishimura, H. and Yano, K., J. Phys. Soc. Japan **57**, 1951 (1988).
8. Hasenburg, H., Bartschat, K., McEachran, R. P. and Stauffer, A. D., J. Phys. B: At. Mol. Phys. **20**, 5165 (1987).
9. Joachain, C. J. and Potvliege, R. M., Phys. Rev. **A35**, 4873 (1987).
10. Bartschat, K., McEachran, R. P. and Stauffer, A. D., J. Phys. B: At. Mol. Phys. **21**, 2789 (1988).
11. Joachain, C. J., Vanderpoorten, R., Winters, K. H. and Byron, F. J., J. Phys. **B10**, 227 (1977).
12. de Heer, F. J., Jansen, R. H. J. and der Kaay, W. V., J. Phys. **B12**, 979 (1979).
13. McCarthy, I. E., Noble, C. J., Phillips, B. A. and Turnbull, A. D., Phys. Rev. **A15**, 2173 (1977).
14. Walters, H. R. J., Phys. Rep. **116**, 1 (1984).
15. Staszewska, G., Schwenke, D. W., Thirumalai, D. and Truhlar, D. G., J. Phys. **B16**, L281 (1983); Phys. Rev. **A28**, 2740 (1983); Staszewaska, G., Schwenke, D. W. and Truhlar, D. G., J. Chem. Phys. **81**, 335 (1984); Phys. Rev. **A29**, 3078 (1983).
16. Jain, A., Phys. Rev. **A34**, 3707 (1986).
17. Hara, S., J. Phys. Soc. Japn **22**, 710 (1967).
18. O'Connell, J. K. and Lane, N. F., Phys. Rev. **A27**, 1893 (1983).
19. Froese-Fischer, C., The Hartree–Fock Method for Atoms. Wiley, New York (1977).
20. Clementi, E. and Roetti, C., At. Data Nucl. Data Tables **14**, 177 (1974).
21. Cox, H. L. Jr. and Bonham, R. A. J., Chem. Phys. **47**, 2599 (1967).
22. Calogero, F., Variable Phase Approach to Potential Scattering. Academic, New York (1967).
23. Nogueira, J. C., Iga, I. and Mu-Tao, L., J. Phys. **B15**, 2539 (1982).
24. Wagenaar, R. W., FOM-Report No. 43948 (1978).
25. Kauppila, W. E., Stein, T. S., Smart, J. H., Dababneh, M. S., Ho, Y. K., Downing, J. P. and Pol, V., Phys. Rev. **A24**, 725 (1981).
26. Dababneh, M. S., Kauppila, W. E., Dowing, J. P., Laperriere, F., Pol, V., Smart, J. H. and Stein, T. S., Phys. Rev. **A22**, 1852 (1980).
27. Dababneh, M. S., Hsieh, Y. F., Kauppila, W. E., Pol, V. and Stein, T. S., Phys. Rev. **A26**, 1252 (1982).
28. Srivastava, S. K., Tanaka, J., Chutjian, A. and Trajmar, S., Phys. Rev. **A23**, 2156 (1981).
29. Williams, J. F. and Willis, B. A., J. Phys. **B8**, 1670 (1975).
30. Williams, J. F. and Crowe, A., J. Phys. **B8**, 2233 (1975).
31. Jansen, J. H. and de Heer, F. J., J. Phys. **B9**, 213 (1976).
32. Jansen, J. H., de Heer, F. J., Luyken, H. L. and van Wingerdon, B., J. Phys. B: At. Mol. Phys. **9**, 185 (1976).
33. Bromberg, J. P., J. Chem. Phys. **61**, 963 (1974).
34. Wagenaar, R. W. and de Heer, F. J., J. Phys. **B13**, 3855 (1980).
35. Dubois, R. D. and Rudd, M. E., J. Phys. B: At. Mol. Phys. **9**, 2657 (1976).
36. Williams, J. F., J. Phys. B: At. Mol. Phys. **12**, 265 (1979).
37. Haberland, R., Fritsche, L. and Noffke, J., Phys. Rev. **A33**, 2305 (1986).
38. Bransden, B. H. and McDowell, M. R. C., Phys. Rep. **46**, 249 (1978).